ISBN: 978-3-95450-247-9 ISSN: 2673-5490 doi: 10.18429/JACoW-IPAC2024-WEPR49

NEAR-INFRARED NOISE IN INTENSE ELECTRON BEAMS*

S. Kladov†, Young-Kee Kim, University of Chicago, Chicago, USA
S. Nagaitsev, Brookhaven National Laboratory, Upton, USA
J. Ruan, D. Broemmelsiek, A. Lumpkin, R. Thurman-Keup, J. Jarvis, A. Saewert,
Fermi National Accelerator Laboratory, Batavia, USA
Z. Huang, SLAC National Accelerator Laboratory, Menlo Park, USA

Abstract

Requirements for the noise in electron beams (NEB) have recently approached the Shot-noise level in some new applications. The density fluctuations of intense beams in the near-infrared (NIR) region are being measured at the Fermilab Accelerator Science and Technology (FAST) facility. The main goal of the experiment is to accurately compare the Shot-noise model with the observations of optical transition radiation (OTR) generated by a relativistic electron beam ($\gamma \approx 63$), transiting an Aluminium metal surface. In addition, some evidence for longitudinal space-charge-induced microbunching for the chicane-compressed beam was obtained with coherent enhancements up to 100 in the various bandwidth-filtered NIR OTR photodiode signals. With micropulse charges up to 1 nC, the beam parameters are close to those proposed for a stage in an Electron-Ion Collider (EIC) with coherent electron cooling (CEC). In this paper we present the current progress of the NEB project and compare the low electron energy measurements with ImpactX simulations.

INTRODUCTION

The relativistic electron-beam quality's importance has become significant as the allowed density fluctuations approached the Poisson level in some applications, including FELs [1, 2] and high-energy hadron storage rings cooling systems [3, 4].

Stochastic cooling is the best option at these energies, and the cooling rate is proportional to the operational frequency of the device [5], which makes the Optical Stochastic Cooling (OSC) orders of magnitude more effective than the microwave stochastic cooling schemes [6]. Coherent Electron Cooling (CEC) is a variation of OSC, where both detector and kicker are the same electron beam [7, 8]: first, it receives a longitudinal kick, shaped in accordance with the hadron beam; then the kick is transformed to longitudinal density modulation by a chicane (amplifier); finally, the hadron beam is kicked by the modulated electron beam with a particular phase shift, thus achieving cooling. The characteristic wavelength of the kick is $\sim 1\ \mu$m. Basic scheme of the system, that will be built at the Electron Ion Collider (EIC), is presented on Fig. 1 [9].

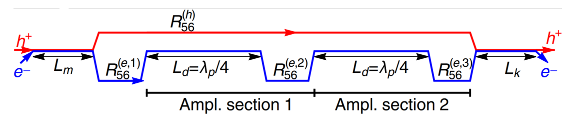

Figure 1: Coherent Electron Cooling (CEC) scheme at Electron Ion Collider (EIC).

Additional beam density modulations in the interesting spectral region introduce additional diffusion in a cooled beam that counteracts cooling [3, 4, 10]. Therefore, if this noise is not controlled at sufficiently low level, the noise heating effects can overcome cooling. The ratio for the EIC can be calculated to be approximately:

$$\frac{D_{\rm diff}}{D_{\rm cool}} = r_2 \frac{\int_{-\infty}^{\infty} \left|Z_{e,2}(k)\right|^2 \left|\delta\rho_e(k)\right|^2 dk}{\int_{-\infty}^{\infty} \left|Z_{e,2}(k)\right|^2 \frac{1}{n_e} dk} = 0.0013F, \quad (1)$$

where r_2 is the ratio for the shot-noise (quiet) beam, $Z_{e,2}(k)$ is the total impedance of the amplifier and kicker sections of CEC for pre-existing electron density modulations $\delta\rho_e(k)$, n_e is the number of electrons in the beam, and $F = n_e \left|\delta\rho_e(k)\right|^2$ is the Fano factor (here we assumed that the noise is white). Noise above shot-level ($F = 1$) in linear electron accelerators without external wavelength modulation has already been observed, for example, in [11].

The Fermilab Accelerator Science and technology (FAST) Facility is well-suited for this research as it can provide electron bunches with similar beam parameters as in the EIC CEC concept. The comparison is presented in Table 1.

In this paper we present the current status of Noise in Electron Beams (NEB) project [12], including measurements of the low energy electron noise for various beam lengths, supported by phase-space simulations.

Table 1: FAST and Proposed CEC Beam Parameters

Parameter	FAST	EIC
E_p, GeV		100 - 275
E_e, MeV	40 - 300	50 - 150
Bunch charge, nC	0 - 3	1
ϵ (rms, norm), μm	3 (at 1 nC)	2.8
Bunch length, mm	0.3 - 10	12 - 8
Drift section, m	80	100

* This manuscript has been authored by Fermi Research Alliance, LLC under Contract No. DE-AC02-07CH11359 with the U.S. Department of Energy, Office of Science, Office of High Energy Physics. Report number is FERMILAB-CONF-24-0261-AD. This work was supported by the U.S. National Science Foundation under Award PHY-1549132, the Center for Bright Beams. This research used the open-source particle-in-cell code ImpactX https://github.com/ECP-WarpX/impactx. We acknowledge all ImpactX contributors.
† kladov@uchicago.edu

ISBN: 978-3-95450-247-9 ISSN: 2673-5490 doi: 10.18429/JACoW-IPAC2024-WEPR49

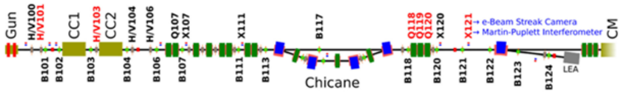

Figure 2: Diagnostics cross X121 is downstream of the chicane upstream of the SRF cryomodule.

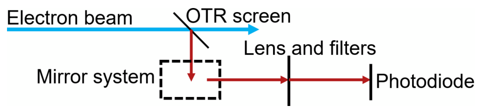

Figure 3: Principal experimental scheme.

METHODS

Density distortions in electron beams are measured by means of Transition Radiation (TR). In FELs, for example, the space charge impedance in a long linear accelerator, as well as strong compression to a high peak current, often result in beam micro-structures [13] that strongly amplify the TR in optical range of frequencies, known as coherent optical transition radiation (COTR) [14].

The TR energy per unit frequency ω per unit solid angle, radiated by a beam of charged particles, traversing an ideal conducting plane, can be approximated as:

$$\frac{d^2 I}{d\omega d\Omega} = \frac{d^2 I_1}{d\omega d\Omega} N^2 \left|\rho(w)\right|^2 = \frac{d^2 I_1}{d\omega d\Omega} N F(w), \quad (2)$$

where N is the number of particles, $\rho(w)$ is the Fourier spectrum of the normalized by 1 longitudinal beam density distribution function, and

$$\frac{d^2 I_1}{d\omega d\Omega} = \frac{Z_0 q^2}{4\pi^3} \frac{\beta^2 \sin^2\theta}{(1-\beta^2\cos^2\theta)^2} \approx \frac{Z_0 q^2}{4\pi^3} \frac{\theta^2}{(\gamma^{-2}+\theta^2)^2}, \quad (3)$$

where $\beta = v/c$, $Z_0 \approx 377\,\Omega$ is the impedance of free space, q is the single particle charge, and the relativistic factor $\gamma \gg 1$. Assuming a bunch charge of 1 nC, the radiation energy per quiet bunch ($F(w) = 1$) in the band $\Delta\lambda = 100$nm, $\lambda_0 = 1\,\mu$m at 25 MeV is 2.4 pJ.

The transverse size dependence, studied in [15, 16], is omitted here due to a different measurement system and its inconsistency with the experimental observations: the exponent presented in the text gives pure zero COTR amplitude for any beam distribution. Instead, we estimate the transverse size impact on COTR as $1/(\lambda/\sigma_\perp)$.

The experiments have been performed using the existing diagnostics cross X121 (see Fig. 2). The principal experimental apparatus, shown in Fig. 3, starts with an Al-coated Si substrate - a thin highly reflective foil (the OTR source), inserted into the beam line at 45 degrees with respect to the beam. The emitted radiation energy is transported through an optical channel, passed through one of the available 12 NIR BPFs filters in the range of 750-2400 nm, and focused onto a sensitive photodiode.

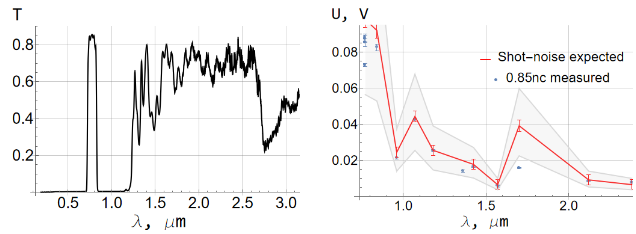

Figure 4: 770nm BP filter transmission function (left), and voltage induced by the OTR radiation for the shot-noise predictions vs measurements (right). X-axis values are the BPFs mean according to the manufacturer.

EXPERIMENTAL RESULTS

The filter transmission functions, an example of which is presented on Fig. 4 left, are far from the desired 100 nm bandwidth ideals. This fact introduces an ambiguity in the transformation from the measured induced voltage to the beam distribution $U_i \rightarrow \rho(\lambda)$. Therefore, we fit the data by repeatedly taking guesses of the distribution:

$$\frac{\text{elevated}}{\text{quiet}} = \frac{\int T(\lambda)F(\lambda)/\lambda^2 d\lambda}{\int T(\lambda)1/\lambda^2 d\lambda} \quad (4)$$

where $F(\lambda) = N\left|\rho(\lambda)\right|^2$ is the Fano factor spectral density and $T(\lambda)$ is the transmission function of the transport line, including the photodiode responsivity.

Comparison of the theoretical predictions and experimental results is presented on Fig. 4 right. Here the combined reflectivity of the light channel is taken to be 80 ± 10 %, and the transverse beam shape - round Gaussian. Red values are the predicted voltages, induced by the radiation passed through the filters; blue values are the measured voltages. Two errors include common and individual multipliers at all points. Individual errors are depicted at both experimental and theoretical curves as error bars, while the common multiplier and systematic errors are shown as bands.

In this case the guess of the Fano factor not depending on the wavelength gives a good agreement with the gain shape. Hence, we can fit the common multiplier directly, obtaining $F = 1 \div 1.7$. At 3σ the factor results in the cooling time being reduced by less than 1%: $T_{\rm diff}/T_{\rm cool} \approx 250$.

If the microbunching wavelength scales the same way as the beam length without amplitude change, it is important to verify that the beam has $F = 1$ in the range $\frac{\lambda}{10\mu m} < c$, where c is the beam compression factor. The increase has been observed in several experiments with external modulation [17, 18], giving peaked gain ($\frac{\rm COTR}{\rm OTR}$), and without a particular excitation [14, 19] with the gain being broad-band and monotonously increasing with wavelength starting at around 200 μm.

Beam length dependence on the CC2 phase relative to the on-crest value, together with its simulated version (see the Simulations section) and the OTR peak, is presented on Fig. 5 left. The maximum compression factor achieved is $c = 0.1$ (from 10 ps to 1 ps), in a small area around

ISBN: 978-3-95450-247-9 ISSN: 2673-5490 doi: 10.18429/JACoW-IPAC2024-WEPR49

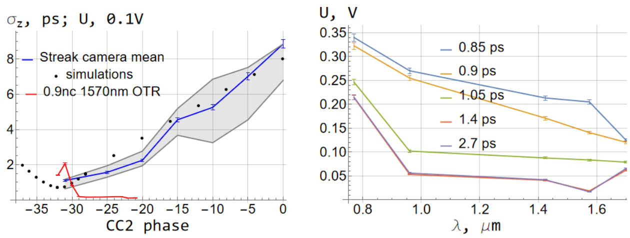

Figure 5: Beam length vs CC2 phase from streak camera, simulations and transition radiation (left), and the elevated signal (right).

which the TR signal appeared to be elevated. The maximum registered signal increase was around 60 times. The OTR signals comparison for various beam lengths is presented on Fig. 5 right.

Because of the absence of an external wavelength in the interesting range, we expect a broad-band spectrum. The task is to fit the data while keeping the peak number as low as possible, and their widths - as large as possible. However, broadband spectra give unexpectedly poor results, predicting much higher gain at 770 nm than it is on the experiment due to the wide transmission range of the filter. Two example of possible fits are presented on Fig. 6. With the factor of $1/(\lambda/\sigma_\perp)$ the diffusion time becomes much lower than the cooling time.

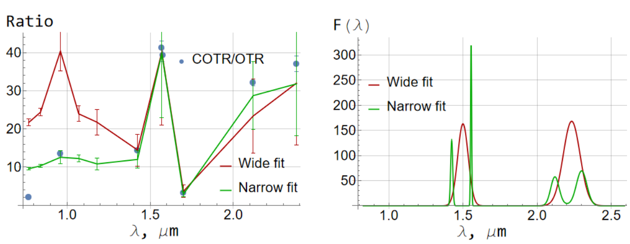

Figure 6: Predictions for the guessed spectrum vs experiment (left), and the guessed Fano factor (right).

It was observed from the signal fluctuations measurements that the incoherent term is not changed when the COTR appears, and the COTR has a random origin. It was also observed from the cavity phase dependence that the microbunching does not depend on the beam length only, but also directly on the acceleration cavity phase.

SIMULATIONS

The space charge tracking, including the intra-microbunch forces, has been done in an s-based ImpactX [20] code on a personal computer.

The simulated set includes initial beam distributions with different-wavelength sinusoidal longitudinal density perturbations. The microbunching gain dependence on the initial beam density perturbation wavelength for various compression factors (CC2 phases) is presented on Fig. 7. The gain at the modulation wavelength is the ratio of the integrals over the final and initial Fano factors. The integration is done in vicinity of the spectrum peaks, that are located near the compressed initial perturbation wavelength $\lambda = c\lambda_0$, where c is the compression factor.

The microbunches are expanded longitudinally on the phase space in the chicane and intersect with each other, achieving smoothing. The effect does not depend on the initial micro-bunch size, and, as a result, the gain quickly approaches 0 with the wavelength and beam length decrease. The low-wavelength area of the compressed beam spectrum is presented on Fig. 8 left. The spectrum mean of the interesting wavelength region is shown as a horizontal line and compared with the shot-noise level. The difference is much smaller than the noise level $F - 1 \ll 1$. An example of the longitudinal phase space after the bunching chicane is presented on Fig. 8 right (Q = 1 nC, λ_0 = 800 nm).

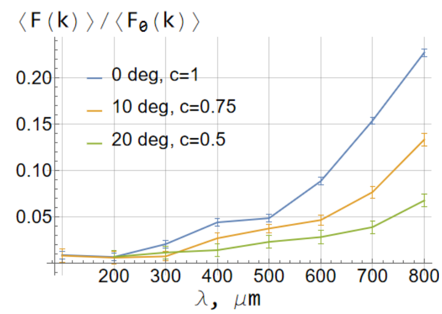

Figure 7: Microbunching gain obtained with ImpactX for the low energy FAST beam line.

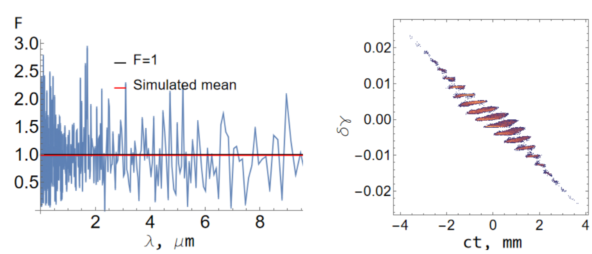

Figure 8: Low-wavelength region of the simulated longitudinal beam distribution spectrum for compressed (1 ps long) beams at low energy (γ=50) FAST beam line (left), and longitudinal phase space after the bunching chicane (right).

CONCLUSION

The experiment shows no additional noise above shot level F = 1 for the uncompressed or moderately compressed beam (l > 2 ps). This result is supported by space-charge particle tracking. At 3σ the cooling time is reduced by less than 1%: $T_{\text{diff}}/T_{\text{cool}} \approx 250$.

On the contrary, the experimentally measured and simulated COTR for compressed beams is clearly in disagreement in the optical and NIR regions. Other possible sourced of the signal increase are Coherent Optical Synchrotron Radiation (COSR) and Coherent Optical Edge Radiation (COER) from the last chicane dipole, both reflected by the OTR screen at X121. COSR and COER simulations are ongoing project activities.

ISBN: 978-3-95450-247-9 ISSN: 2673-5490 doi: 10.18429/JACoW-IPAC2024-WEPR49

REFERENCES

[1] Z. Huang and K.-J. Kim, "Review of x-ray free-electron laser theory," *Phys. Rev. Spec. Top. Accel. Beams*, vol. 10, p. 034801, Mar 2007. doi:10.1103/PhysRevSTAB.10.034801

[2] E. Saldin, E. Schneidmiller, and M. Yurkov, "Study of a noise degradation of amplification process in a multistage hghg fel," *Opt. Commun.*, vol. 202, no. 1, pp. 169–187, 2002. doi:10.1016/S0030-4018(02)01091-X

[3] G. Stupakov and P. Baxevanis, "Microbunched electron cooling with amplification cascades," *Phys. Rev. Accel. Beams*, vol. 22, p. 034401, Mar 2019. doi:10.1103/PhysRevAccelBeams.22.034401

[4] W. Bergan, "Electron diffusion in microbunched electron cooling," 2024. doi:10.48550/arXiv:2403.17721

[5] V. Lebedev, "High energy cooling," 2024. doi:10.48550/arXiv:2401.15091

[6] M. S. Zolotorev and A. A. Zholents, "Transit-time method of optical stochastic cooling," *Phys. Rev. E*, vol. 50, pp. 3087–3091, Oct. 1994. doi:10.1103/PhysRevE.50.3087

[7] V. N. Litvinenko and Y. S. Derbenev, "Coherent electron cooling," *Phys. Rev. Lett.*, vol. 102, p. 114801, Mar. 2009. doi:10.1103/PhysRevLett.102.114801

[8] D. Ratner, "Microbunched electron cooling for high-energy hadron beams," *Phys. Rev. Lett.*, vol. 111, p. 084802, Aug. 2013. doi:10.1103/PhysRevLett.111.084802

[9] F. Willeke and J. Beebe-Wang, "Electron ion collider conceptual design report 2021," , Brookhaven National Lab, Upton, NY, USA, Tech. Rep. BNL-221006-2021-FORE, 2021. doi:10.2172/1765663

[10] G. Stupakov, "Cooling rate for microbunched electron cooling without amplification," *Phys. Rev. Accel. Beams*, vol. 21, p. 114402, Nov 2018. doi:10.1103/PhysRevAccelBeams.21.114402

[11] A. Gover, A. Nause, E. Dyunin, and M. Fedurin, "Beating the shot-noise limit," *Nat. Phys.*, vol. 8, no. 12, pp. 877–880, 2012. doi:10.1038/nphys2443

[12] S. Nagaitsev *et al.*, "Noise in Intense Electron Bunches", in *Proc. NAPAC'22*, Albuquerque, NM, USA, Aug. 2022, pp. 128–131. doi:10.18429/JACoW-NAPAC2022-MOPA34

[13] Z. Huang and G. Stupakov, "Control and application of beam microbunching in high brightness linac-driven free electron lasers," *Nucl. Instrum. Methods Phys. Res., Sect. A*, vol. 907, pp. 182–187, 2018. doi:10.1016/j.nima.2018.02.030

[14] H. Loos *et al.*, "Observation of coherent optical transition radiation in the lcls linac," *30th International Free Electron Laser Conference, FEL 2008*, Gyeongju, South Korea, Aug. 2008, pp. 485–489.

[15] G. L. Orlandi, "Spatial coherence in the transition radiation spectrum," *Opt. Commun.*, vol. 267, no. 2, pp. 322–334, 2006. doi:10.1016/j.optcom.2006.06.056

[16] E. Chiadroni, M. Castellano, A. Cianchi, K. Honkavaara, and G. Kube, "Effects of transverse electron beam size on transition radiation angular distribution," *Nucl. Instrum. Methods Phys. Res., Sect. A*, vol. 673, pp. 56–63, 2012. doi:10.1016/j.nima.2012.01.011

[17] A. H. Lumpkin, R. J. Dejus, and N. S. Sereno, "Coherent optical transition radiation and self-amplified spontaneous emission generated by chicane-compressed electron beams," *Phys. Rev. ST Accel. Beams*, vol. 12, p. 040704, Apr 2009. doi:10.1103/PhysRevSTAB.12.040704

[18] A. Tremaine *et al.*, "Observation of self-amplified spontaneous-emission-induced electron-beam microbunching using coherent transition radiation," *Phys. Rev. Lett.*, vol. 81, pp. 5816–5819, Dec 1998. doi:10.1103/PhysRevLett.81.5816

[19] S. Wesch, C. Behrens, B. Schmidt, and P. Schmüser, "Observation of coherent optical transition radiation and evidence for microbunching in magnetic chicanes," in *Proc. 31st Int. Free Electron Laser Conf.(FEL'09)*, Liverpool, UK, Aug. 2009, pp. 619–622.

[20] A. Huebl *et al.*, "Next generation computational tools for the modeling and design of particle accelerators at exascale," 2022. doi:10.48550/arXiv:2208.02382